2018 European Control Conference (ECC)
June 12-15, 2018. Limassol, Cyprus

An Algorithm for Mixed-Integer Optimal Control of Solar Thermal Climate Systems with MPC-Capable Runtime

Adrian Bürger[1,2], Clemens Zeile[3], Angelika Altmann-Dieses[1], Sebastian Sager[3], Moritz Diehl[2,4]

Abstract— **This work presents an algorithm for solution of Mixed-Integer Optimal Control Problems (MIOCPs) for Solar Thermal Climate Systems (STCSs) with MPC-capable runtime. We implement the so-called Combinatorial Integral Approximation (CIA) algorithm for a model of an STCS of a building that incorporates an adsorption cooling machine and apply the algorithm within a numerical case study to solve a Mixed-Integer Non-Linear Program (MINLP) resulting from an MIOCP for the system. We compare the results of the CIA algorithm to those of a general MINLP solver and show that our algorithm achieves comparable solution quality at a runtime that is up to 1000 times smaller.**

I. Introduction

Energy consumption of buildings accounts for up to 40 % of the total energy consumption of some developed countries [1]. Major shares of this energy are used within Heating, Ventilation and Air Conditioning (HVAC), while worldwide more energy is consumed for cooling energy production than for space heating [1]. In contrast to conventional cooling devices driven by electrical energy, technologies like adsorption cooling can utilize low temperature heat like waste heat of industrial processes and solar heat as driving energy for the cooling process, and with this, facilitate more ecological cooling energy production [2], [3].

Both operability and efficiency of an Adsorption Cooling Machine (ACM) highly depend on its current operation conditions regarding driving energy temperature and recooling temperature [3]. When driving ACMs with waste heat or solar thermal energy, energy occurrences can possibly be predicted in the form of, e. g., production plans or weather forecasts. This favors the use of optimization-based control methods, where forecasts can be taken into account directly for predictive control decisions that facilitate efficient ACM operation.

Within MPC for ACMs, the subject of optimization can either be the machine's internal processes [4], [5] or the optimized scheduling of an ACM of determined behavior [6]. In this work, we focus on the second case and optimize the switching of an ACM depending on the predicted operation conditions. In presence of additional, continuous optimization variables such as mass flow rates, the optimization problem becomes a Mixed-Integer Optimal Control Problem (MIOCP) [7].

For the solution of Optimal Control Problems (OCPs) in general and for the special case of MIOCPs, the use of direct methods and especially of direct multiple shooting or direct collocation is favorable [7], [8]. For the case of MIOCPs, this results in Mixed-Integer Non-Linear Programs (MINLPs). General MINLP algorithms and according numerical solvers exist to solve these problems, e. g., the open-source solver Bonmin [9]. However, these solvers that aim to solve the exact MINLP tend to work only on small time horizons, since the problem complexity and with this also the potential solver runtime increases exponentially with the number of discrete time points. This renders these methods less favorable for use within real-time MPC applications where solution speed is crucial [7]. Therefore, it was proposed to decompose the MINLP into a Non-Linear Program (NLP) and a Mixed-Integer Linear Program (MILP) [10], [11]. This approach, further referred to as Combinatorial Integral Approximation (CIA), is justified by error bounds depending on the discretization grid and has been successfully applied to, e. g., water networks [12] and vehicle driving [13].

Within this work, we implement a CIA algorithm for a model of a Solar Thermal Climate System (STCS) installed at Karlsruhe University of Applied Sciences that incorporates an ACM. Since the separate optimization of the ACM switching can result in situations where the machine's scheduled operation times do not match the optimized profile of the continuously controllable mass flow rates, we implement a subsequent NLP solution step as proposed in [11] to avoid possible operation efficiency losses or even harmful operating modes. The implemented algorithm is tested within a numerical case study and the solutions are compared to the results of Bonmin in terms of solution quality, runtime and coverage of combinatorial, vanishing and slack variable induced constraints. The algorithm is shown to achieve results of comparable quality at a runtime that is up to 1000 times smaller and suitable for application within MPC of climate systems.

The paper is structured as follows: In Section II, the STCS considered within this study and the modeling approach for the system are described. In Section III, the CIA algorithm used within this work is introduced. The implementation of the algorithm for the STCS is illustrated in Section IV and the results of an application for multiple test scenarios are evaluated. Section V concludes and suggests future work.

[1] Faculty of Management Science and Engineering, Karlsruhe University of Applied Sciences, Germany. Email: {adrian.buerger, angelika.altmann-dieses}@hs-karlsruhe.de
[2] Systems Control and Optimization Laboratory, Department of Microsystems Engineering (IMTEK), University of Freiburg, Germany. Email: moritz.diehl@imtek.uni-freiburg.de
[3] MathOpt Group, Institute for Mathematical Optimization, Faculty of Mathematics, Otto-von-Guericke University Magdeburg, Germany. Email: {clemens.zeile, sager}@ovgu.de
[4] Department of Mathematics, University of Freiburg, Germany.

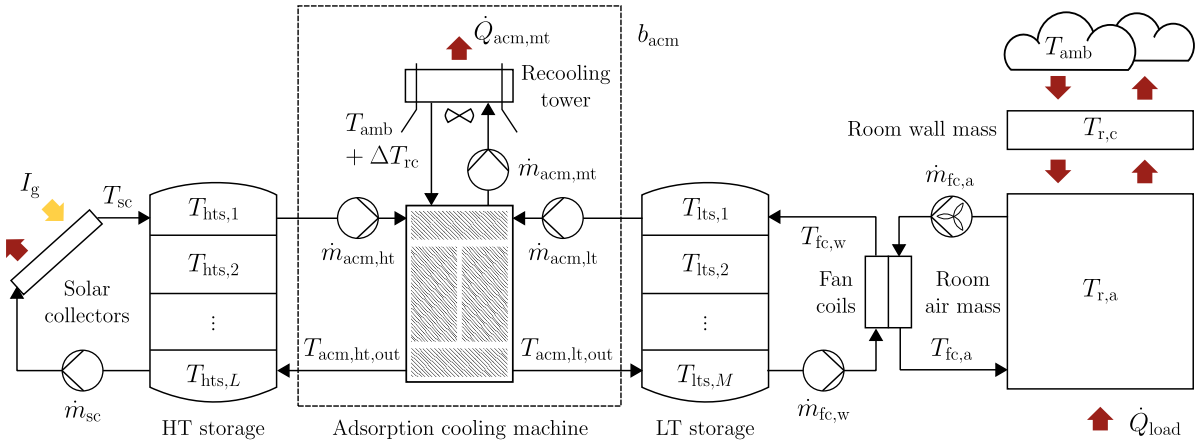

Fig. 1. Depiction of the STCS considered within this study. Red arrows indicate heat exchange, yellow arrows indicate solar irradiation.

II. Solar Thermal Climate System

A. System description and control objective

A depiction of the STCS considered within this study, which is installed at the Faculty of Management Science and Engineering at Karlsruhe University of Applied Sciences, is given in Fig. 1. It models an array of horizontally placed solar thermal collectors with total collector surface $A_{\mathrm{sc}} = 35.0\,\mathrm{m}^2$ and optical efficiency $\eta_{\mathrm{sc}} = 0.7$ that supports a stratified High Temperature (HT) water storage of volume $V_{\mathrm{hts}} = 2.0\,\mathrm{m}^3$. The water mass flow rate $\dot{m}_{\mathrm{sc}}$ through the collectors[1] can be set on a continuous scale $\dot{m}_{\mathrm{sc}} \in [0, 0.5]\,\mathrm{kg/s}$.[2] The hot water from the top of the HT storage can be utilized for operation of a silica-gel/water ACM which, when switched on ($b_{\mathrm{acm}} = 1$), utilizes the heat from the HT storage to absorb heat from a stratified Low Temperature (LT) water storage with volume $V_{\mathrm{lts}} = 1.0\,\mathrm{m}^3$ and emits the combined heat through a recooling tower.

The water from the bottom of the LT storage can be used to support a set of fan coils that are operated for heat exchange with the air mass $m_{\mathrm{r,a}} = 2.16 \cdot 10^3\,\mathrm{kg}$ of a room. The water mass flow rate $\dot{m}_{\mathrm{fc,w}}$ through the fan coils can be set on a continuous scale $\dot{m}_{\mathrm{fc,w}} \in [0, 0.3]\,\mathrm{kg/s}$, the air mass flow rate $\dot{m}_{\mathrm{fc,a}} = 0.43\,\mathrm{kg/s}$ through the fan coils is assumed constant.[3] The room air also exchanges heat with the concrete wall mass $m_{\mathrm{r,c}} = 2.376 \cdot 10^5\,\mathrm{kg}$ of temperature $T_{\mathrm{r,c}}$, which in turn exchanges heat with the environment depending on the ambient temperature T_{amb}.

The room temperature $T_{\mathrm{r,a}}$ is affected by a time-varying heat load $\dot{Q}_{\mathrm{load}}$ that is due to influences from heating through solar irradiation on the building and internal heat loads from machines and humans. The control objective for the system is to keep the room's air temperature $T_{\mathrm{r,a}}$ within a defined comfort range.

B. Modeling approach

The models used within this study are gray-box models of system components based on mass and energy balances. They fulfill all necessary conditions regarding differentiability that enables further use within derivative-based optimization methods, cf. [14]. The ACM and storage models have been used successfully in a previous study [6]. Energy losses to the environment are neglected except for room wall and solar collectors. All materials and media within the system are assumed to be incompressible and with constant specific heat capacities and densities as given in Table I.

1) Solar collector model: A single-node solar collector model is used to calculate the collector temperature T_{sc} as

$$\begin{aligned}\dot{T}_{\mathrm{sc}}(t) = C_{\mathrm{sc}}^{-1}[&\dot{m}_{\mathrm{sc}}(t) c_{\mathrm{w}} (T_{\mathrm{hts},L}(t) - T_{\mathrm{sc}}(t)) \\ &+ \eta_{\mathrm{sc}} A_{\mathrm{sc}} I_{\mathrm{g}}(t) - \alpha_{\mathrm{sc}} A_{\mathrm{sc}} (T_{\mathrm{sc}}(t) - T_{\mathrm{amb}}(t))]\end{aligned} \tag{1}$$

with $C_{\mathrm{sc}} = 2.6\,\mathrm{kJ/K}$ the heat capacity of the solar collectors including the contained medium and $\alpha_{\mathrm{sc}} = 1.4\,\mathrm{W/(m^2K)}$ the heat transfer coefficient for the heat losses, cf. [15].

2) HT water storage: The volume V_{hts} of the stratified storage tank is discretized into $L = 4$ layers and an energy balance is calculated for each layer to determine its temperature, cf. [16], [17], [6]. The occurrence of mass flows between storage layers depends on the current value of $\dot{m}_{\mathrm{sc}}$ and the ACM operation status $b_{\mathrm{acm}} \in \{0, 1\}$. Using the water mass of a layer $m_{\mathrm{hts}} = (\rho_{\mathrm{w}} V_{\mathrm{hts}})/L = 500\,\mathrm{kg}$ and assuming $\dot{m}_{\mathrm{sc}}(t) < \dot{m}_{\mathrm{acm,ht}}$, the energy balance that determines the

TABLE I
Specific heat capacities and densities of materials and media

Substance	Specific heat capacity	Density
Water	$c_{\mathrm{w}} = 4.12\,\mathrm{kJ/(kgK)}$	$\rho_{\mathrm{w}} = 10^3\,\mathrm{kg/m^3}$
Air	$c_{\mathrm{a}} = 1.005\,\mathrm{kJ/(kgK)}$	$\rho_{\mathrm{a}} = 1.2\,\mathrm{kg/m^3}$
Concrete	$c_{\mathrm{c}} = 0.88\,\mathrm{kJ/(kgK)}$	$\rho_{\mathrm{c}} = 2.2 \cdot 10^3\,\mathrm{kg/m^3}$

[1] Usual system separations of outdoor circuits containing, e. g., glycol-water-mixtures from indoor water circuits are neglected for simplicity.

[2] Within this study, we assume that additional, low-level controllers can translate the mass flow rates requested by the high-level system controller into corresponding pump speeds, and neglect minimum pump flow rates.

[3] In the real application, a constant operation of fan coils which we assume here for simplicity would be inefficient. However, the operation of the fan coils could be set depending on pump operation, so that the fans are activated only when the pump is working, which results in a similar system behavior.

temperature $T_{\mathrm{hts},1}$ of the top layer can be calculated as

$$\begin{aligned}\dot{T}_{\mathrm{hts},1}(t) = m_{\mathrm{hts}}^{-1}[&\dot{m}_{\mathrm{sc}}(t)T_{\mathrm{sc}}(t)\\ &-(1-b_{\mathrm{acm}}(t))\dot{m}_{\mathrm{sc}}(t)T_{\mathrm{hts},1}(t)\\ &+b_{\mathrm{acm}}(t)(\dot{m}_{\mathrm{acm,ht}}-\dot{m}_{\mathrm{sc}}(t))T_{\mathrm{hts},2}(t)\\ &-b_{\mathrm{acm}}(t)\dot{m}_{\mathrm{acm,ht}}T_{\mathrm{hts},1}(t)].\end{aligned} \tag{2}$$

The energy balance for each middle layer $k = 2, \ldots, L-1$ is given in (3) and for the bottom layer in (4).

$$\begin{aligned}\dot{T}_{\mathrm{hts},k}(t) = m_{\mathrm{hts}}^{-1}[&(1-b_{\mathrm{acm}}(t))\dot{m}_{\mathrm{sc}}(t)T_{\mathrm{hts},k-1}(t)\\ &-b_{\mathrm{acm}}(t)(\dot{m}_{\mathrm{acm,ht}}-\dot{m}_{\mathrm{sc}}(t))T_{\mathrm{hts},k}(t)\\ &+b_{\mathrm{acm}}(t)(\dot{m}_{\mathrm{acm,ht}}-\dot{m}_{\mathrm{sc}}(t))T_{\mathrm{hts},k+1}(t)\\ &-(1-b_{\mathrm{acm}}(t))\dot{m}_{\mathrm{sc}}(t)T_{\mathrm{hts},k}(t)]\end{aligned} \tag{3}$$

$$\begin{aligned}\dot{T}_{\mathrm{hts},L}(t) = m_{\mathrm{hts}}^{-1}[&-\dot{m}_{\mathrm{sc}}(t)T_{\mathrm{hts},L}(t)\\ &+(1-b_{\mathrm{acm}}(t))\dot{m}_{\mathrm{sc}}(t)T_{\mathrm{hts},L-1}(t)\\ &+b_{\mathrm{acm}}(t)\dot{m}_{\mathrm{acm,ht}}T_{\mathrm{acm,ht,out}}(t)\\ &-b_{\mathrm{acm}}(t)(\dot{m}_{\mathrm{acm,ht}}-\dot{m}_{\mathrm{sc}}(t))T_{\mathrm{hts},L}(t)]\end{aligned} \tag{4}$$

3) Adsorption cooling machine and recooling tower: We assume the temperature of the medium supplied by the recooling tower to be of a constant difference ΔT_{rc} to the current ambient temperature T_{amb}. Given valid inlet temperature configurations for ACM operation, the mean cooling power $\dot{Q}_{\mathrm{acm,lt}}$ and the mean Coefficient Of Performance (COP) of an ACM during an adsorption cycle is determined. According data can, e. g., be obtained from measurements or machine data sheets. From suitable (polynomial) curve fittings $f_{\dot{Q}_{\mathrm{acm,lt}}}(\cdot)$ and $f_{\mathrm{cop}}(\cdot)$ to these data, energy balances for the machine's three circuits can be calculated as in

$$\begin{aligned}\dot{Q}_{\mathrm{acm,lt}}(t) &= f_{\dot{Q}_{\mathrm{acm,lt}}}(T_{\mathrm{hts},1}(t), T_{\mathrm{lts},1}(t), T_{\mathrm{amb}}(t)),\\ \dot{Q}_{\mathrm{acm,ht}}(t) &= \frac{\dot{Q}_{\mathrm{acm,lt}}(t)}{f_{\mathrm{cop}}(T_{\mathrm{hts},1}(t), T_{\mathrm{lts},1}(t), T_{\mathrm{amb}}(t))},\\ \dot{Q}_{\mathrm{acm,mt}}(t) &= \dot{Q}_{\mathrm{acm,lt}}(t) + \dot{Q}_{\mathrm{acm,ht}}(t).\end{aligned} \tag{5}$$

Low Medium Temperature (MT) input temperatures and high HT and LT input temperatures are favorable conditions for efficient operation of the ACM [3]. Using (5), the mean output temperatures of the ACM can be calculated as

$$\begin{aligned}T_{\mathrm{acm,lt,out}}(t) &= T_{\mathrm{lts},1}(t) - \frac{\dot{Q}_{\mathrm{acm,lt}}(t)}{c_{\mathrm{w}}\dot{m}_{\mathrm{acm,lt}}},\\ T_{\mathrm{acm,ht,out}}(t) &= T_{\mathrm{hts},1}(t) - \frac{\dot{Q}_{\mathrm{acm,ht}}(t)}{c_{\mathrm{w}}\dot{m}_{\mathrm{acm,ht}}},\\ T_{\mathrm{acm,mt,out}}(t) &= T_{\mathrm{amb}}(t) + \Delta T_{\mathrm{rc}} + \frac{\dot{Q}_{\mathrm{acm,mt}}(t)}{c_{\mathrm{w}}\dot{m}_{\mathrm{acm,mt}}},\end{aligned} \tag{6}$$

using the mass flow rates $\dot{m}_{\mathrm{acm,lt}} = 48\,\mathrm{kg/min}$, $\dot{m}_{\mathrm{acm,ht}} = 41.8\,\mathrm{kg/min}$ and $\dot{m}_{\mathrm{acm,mt}} = 85\,\mathrm{kg/min}$. Though the cyclic output temperature behavior of an ACM is not covered by this model, it becomes applicable due to the storages connected to the HT and LT side of the machine and the comparatively high mass flow rate of the MT circuit which dampen the effect of fluctuating output temperatures, see [18], [6].

4) LT water storage: The LT storage model (7) is formulated analogously to the HT storage model using $M = 3$ layers and mass flow rates and temperatures of fan coils and ACM LT circuit. A detailed depiction is omitted for brevity.

$$\begin{aligned}\dot{T}_{\mathrm{lts},1}(t) &= f_{\mathrm{lts},1}(T_{\mathrm{fc,w}}(t), T_{\mathrm{lts},\{1,2\}}(t), \dot{m}_{\mathrm{fc,w}}(t), b_{\mathrm{acm}}(t))\\ \dot{T}_{\mathrm{lts},2}(t) &= f_{\mathrm{lts},2}(T_{\mathrm{lts},\{1,2,3\}}(t), \dot{m}_{\mathrm{fc,w}}(t), b_{\mathrm{acm}}(t))\\ \dot{T}_{\mathrm{lts},3}(t) &= f_{\mathrm{lts},3}(T_{\mathrm{acm,lt,out}}(t), T_{\mathrm{lts},\{2,3\}}(t),\\ &\qquad \dot{m}_{\mathrm{fc,w}}(t), b_{\mathrm{acm}}(t))\end{aligned} \tag{7}$$

5) Fan coil and room models: The model of the fan coils is a single-node model of a gas-liquid heat exchanger with heat transfer coefficient $(A\alpha)_{\mathrm{fc}} = 475\,\mathrm{W/K}$. The temperatures of the water side $T_{\mathrm{fc,w}}$ and the air side $T_{\mathrm{fc,a}}$ are calculated according to (8) with $m_{\mathrm{fc,w}} = 3.6\,\mathrm{kg}$ the water mass and $m_{\mathrm{fc,a}} = 0.198\,\mathrm{kg}$ the air mass inside the fan coil.

$$\begin{aligned}\dot{T}_{\mathrm{fc,w}}(t) &= \frac{\dot{m}_{\mathrm{fc,w}}(t)c_{\mathrm{w}}(T_{\mathrm{lts},M}(t) - T_{\mathrm{fc,w}}(t)) + \dot{Q}_{\mathrm{fc}}(t)}{m_{\mathrm{fc,w}}c_{\mathrm{w}}}\\ \dot{T}_{\mathrm{fc,a}}(t) &= \frac{\dot{m}_{\mathrm{fc,a}}(t)c_{\mathrm{a}}(T_{\mathrm{r,a}}(t) - T_{\mathrm{fc,a}}(t)) - \dot{Q}_{\mathrm{fc}}(t)}{m_{\mathrm{fc,a}}c_{\mathrm{a}}}\\ \dot{Q}_{\mathrm{fc}}(t) &= (A\alpha)_{\mathrm{fc}}(T_{\mathrm{fc,a}}(t) - T_{\mathrm{fc,w}}(t))\end{aligned} \tag{8}$$

The model for the room's air mass temperature $T_{\mathrm{r,a}}$ and the wall's concrete mass temperature $T_{\mathrm{r,c}}$ is a single-node model given in (9). Heat exchange between air and concrete depends on the wall surface $A_{\mathrm{c}} = 540\,\mathrm{m}^2$ and a heat transfer coefficient $\alpha_{\mathrm{a,c}} = 1.5\,\mathrm{W/(m^2K)}$.

$$\begin{aligned}\dot{T}_{\mathrm{r,a}}(t) &= \frac{\dot{m}_{\mathrm{fc,a}}(t)c_{\mathrm{a}}(T_{\mathrm{fc,a}}(t) - T_{\mathrm{r,a}}(t)) + \dot{Q}_{\mathrm{r,i}}(t)}{m_{\mathrm{r,a}}c_{\mathrm{a}}}\\ \dot{T}_{\mathrm{r,c}}(t) &= \frac{A_{\mathrm{c}}\alpha_{\mathrm{a,c}}(T_{\mathrm{amb}}(t) - T_{\mathrm{r,c}}(t)) - \dot{Q}_{\mathrm{r,i}}(t)}{m_{\mathrm{r,c}}c_{\mathrm{c}}}\\ \dot{Q}_{\mathrm{r,i}}(t) &= A_{\mathrm{c}}\alpha_{\mathrm{a,c}}(T_{\mathrm{r,c}}(t) - T_{\mathrm{r,a}}(t))\end{aligned} \tag{9}$$

6) Operation conditions and constraints: The time-varying profiles for ambient temperature T_{amb}, global solar irradiation I_{g} and heat load $\dot{Q}_{\mathrm{load}}$ are assumed as known at all times. System temperatures must neither exceed $T_{\mathrm{ub}} = 110\,^{\circ}\mathrm{C}$ nor go below $T_{\mathrm{lb}} = 5\,^{\circ}\mathrm{C}$. The temperature boundaries for ACM operation are given in Table II.

III. Mixed-integer optimal control

Within this section, we first introduce a generic MIOCP statement. On that basis, we introduce the chosen discretization and CIA solution approach, followed by a more detailed description of the binary control approximation method.

TABLE II
Temperature boundaries for ACM operation

Temperature	Lower bound	Upper bound
$T_{\mathrm{lts},1}$	$T_{\mathrm{lt,lb}} = 10\,^{\circ}\mathrm{C}$	$T_{\mathrm{lt,ub}} = 22\,^{\circ}\mathrm{C}$
$T_{\mathrm{hts},1}$	$T_{\mathrm{ht,lb}} = 55\,^{\circ}\mathrm{C}$	$T_{\mathrm{ht,ub}} = 95\,^{\circ}\mathrm{C}$
T_{amb}	$T_{\mathrm{amb,lb}} = 14\,^{\circ}\mathrm{C}$	$T_{\mathrm{amb,ub}} = 36\,^{\circ}\mathrm{C}$

A. Problem statement

Let $\vec{x}(t) \in \mathbb{R}^{n_x}$ be the differential states, $\vec{u}(t) \in \mathbb{R}^{n_u}$ the continuous controls, $b(t) \in \{0,1\}$ the binary control, $\vec{s}(t) \in \mathbb{R}^{n_s}$ a vector of slack variables and $\vec{c} \in \mathbb{R}^{n_c}$ time-varying parameters with $n_x, n_u, n_s, n_c \in \mathbb{N}$ and $t \in [t_0, t_f] \subset \mathbb{R}$ element of a given time horizon. We minimize the sum of the continuous-time Lagrangian cost functional $L(\cdot)$, which is assumed to be integrable on the time horizon, and the Mayer term $M(\cdot)$. Function $\vec{f}(\cdot)$ describes the right hand side of the differential equations and $\vec{r}(\cdot)$ describes path constraints with lower bound $\vec{r}_{\text{lb}}$ and upper bound $\vec{r}_{\text{ub}}$ that can be relaxed by making use of $\vec{s}$. The functions $\vec{f}(\cdot)$ and $\vec{r}(\cdot)$ are assumed to be continuously differentiable in all arguments within the domain of interest. Lastly, $\mathcal{X}$ and $\mathcal{U}$ denote the feasible domains of the states and the continuous controls, respectively. With $\vec{x}_0 \in \mathbb{R}^{n_x}$ the initial state vector and $\vec{v}(t)^\top = [\vec{x}(t)^\top \vec{u}(t)^\top b(t) \ \vec{s}(t)^\top]$ the vector of optimization variables, the general problem reads as

$$\min_{\vec{v}(\cdot)} \int_{t_0}^{t_f} L(t, \vec{x}(t), \vec{u}(t), b(t), \vec{s}(t)) \, \mathrm{d}t + M(\vec{x}(t_f)) \quad (10a)$$

s.t. for $t \in [t_0, t_f]$:

$$\dot{\vec{x}}(t) = \vec{f}(\vec{x}(t), \vec{u}(t), b(t), \vec{c}(t)), \quad (10b)$$

$$\vec{r}_{\text{lb}} \leq r(t, \vec{x}(t), \vec{u}(t), b(t), \vec{s}(t), \vec{c}(t)) \leq \vec{r}_{\text{ub}}, \quad (10c)$$

$$\vec{x}(t_0) = \vec{x}_0, \quad (10d)$$

$$\vec{x}(t) \in \mathcal{X}, \quad \vec{u}(t) \in \mathcal{U}, \quad b(t) \in \{0,1\}. \quad (10e)$$

B. Problem discretization and CIA approach

Using a *first discretize, then optimize* approach [7], we introduce a discretization grid $\mathcal{G}_N$, divide the time horizon in N control intervals and apply the direct collocation method on this grid, so that the system dynamics (10b) and the path constraints (10c) are reformulated into mixed-integer nonlinear equations and inequalities, respectively. Altogether, this discretization step reformulates the MIOCP into an MINLP. For further details regarding direct collocation we refer to [14].

Since MINLPs are often (very) hard to solve, there exist a variety of solution methods [19]. Due to its specific problem structure, the CIA decomposition approach has been proposed to solve discretized MIOCPs [10], [11]. The idea is to solve a relaxed MINLP, which is an NLP, before approximating the relaxed controls with binary controls, which turns out to be an MILP.

Considering the approximated binary control profile, the continuous controls optimized within the first NLP are not necessarily optimal or even valid anymore regarding control objective and constraints. Therefore, we solve the NLP again with the binary controls fixed in order to adjust the continuous controls to the obtained binary solution. To achieve feasibility, it might be necessary for the optimizer to relax the path constraints via slack variables if (due to the determined binary controls) a feasible solution cannot be obtained from adjustment of the continuous controls alone.

Algorithm 1 summarizes the steps of the CIA algorithm. Note that the discretized MIOCP is the aforementioned MINLP and by relaxing the integrality constraint for $\vec{b}$ from $b \in \{0,1\}$ to $b \in [0,1]$ for all $b \in \vec{b}$, we obtain (NLP). $\vec{b}$ is then discretized on N intervals, unlike in the MIOCP, and reads therefore as a vector. (NLP) is assumed to be solved by an NLP solver, e.g., Ipopt [20].

Algorithm 1: CIA algorithm for MIOCP

Input : Discretized (MIOCP) instance with grid $\mathcal{G}_N$, initial guesses for $\vec{x}, \vec{u}, \vec{b}$.

Output: (Local) Optimal variables $\vec{x}^*, \vec{u}^*, \vec{b}^*, \vec{s}^*$ with objective $\mathcal{L}^* = \mathcal{L}(\vec{x}^*, \vec{u}^*, \vec{b}^*, \vec{s}^*)$.

1 Initialize $\vec{s} = \vec{0}$ and solve (NLP) $\rightarrow$ $\vec{x}$, $\vec{u}$, $\vec{b}_{\text{rel}}$, $\vec{s}$, $\mathcal{L}_{\text{rel}}$.
2 **if** $\vec{b}_{\text{rel}} \in \{0,1\}^N$ **then**
3 | **return**: $(\vec{x}^*, \vec{u}^*, \vec{b}^*, \vec{s}^*, \mathcal{L}^*) = (\vec{x}, \vec{u}, \vec{b}_{\text{rel}}, \vec{s}, \mathcal{L}_{\text{rel}})$;
4 **else**
5 | Solve binary control approximation for $\vec{b}_{\text{rel}} \rightarrow \vec{b}_{\text{bin}}$;
6 | Solve (NLP) with $\vec{b} = \vec{b}_{\text{bin}}$ fixed $\rightarrow$ $\vec{x}$, $\vec{u}$, $\vec{s}$, $\mathcal{L}_{\text{bin}}$;
7 | **return**: $(\vec{x}^*, \vec{u}^*, \vec{b}^*, \vec{s}^*, \mathcal{L}^*) = (\vec{x}, \vec{u}, \vec{b}_{\text{bin}}, \vec{s}, \mathcal{L}_{\text{bin}})$;
8 **end**

If this procedure is repeated with an iteratively refined discretization grid, the achieved solution is going to be arbitrarily close to its relaxed solution. In the following, we refer to Step 1 of Algorithm 1 as $\text{CIA}_{\text{NLP},1}$, Step 5 as CIA_{MILP} and Step 6 as $\text{CIA}_{\text{NLP},2}$. The binary control approximation problem that plays an important role in our algorithm is illustrated in the upcoming subsection.

C. Binary control approximation

A theorem by Sager et al. [10] supports bounds for the rounding error, when solving first the NLP and then approximating the binary controls. Furthermore, it suggests to minimize the maximal accumulated difference of relaxed and binary controls in integral sense. Formulated as a mathematical term and in the MIOCP setting it reads as

$$\min_{b_{\text{bin}}(\cdot)} \max_{t \in [t_0, t_f]} \| \int_{t_0}^{t} b_{\text{rel}}(\tau) - b_{\text{bin}}(\tau) \mathrm{d}\tau \|. \quad (11)$$

If we discretize the controls, it results

$$\min_{\vec{b}_{\text{bin}}} \max_{j \in \mathcal{G}_N} \left| \sum_{i=t_0}^{j} (b_{i,\text{rel}} - b_{i,\text{bin}}) \cdot \Delta t_i \right|, \quad (12)$$

with $\Delta t_i := t_{i+1} - t_i, \ t_i, t_{i+1} \in \mathcal{G}_N$ which can be formulated as an MILP and solved using an MILP solver, or solved directly using a tailored Branch and Bound algorithm [10].

IV. Implementation and application

Within this section, we give a description of the MIOCP formulation for the STCS introduced in Section II and details on software implementation. Afterwards, the results of the application of the algorithms for selected scenarios are discussed.

A. Optimal control problem formulation

In order to adapt the MIOCP formulation to our HVAC system, we first recognize our differential states

$$\vec{x}^\top = [T_{\mathrm{hts},\{1,2,3,4\}}\ T_{\mathrm{lts},\{1,2,3\}}\ T_{\mathrm{sc}}\ T_{\mathrm{fc},\{\mathrm{w,a}\}}\ T_{\mathrm{r},\{\mathrm{a,c}\}}], \quad (13)$$

continuous controls $\vec{u}^\top = [\dot{m}_{\mathrm{sc}}\ \dot{m}_{\mathrm{fc,w}}]$ and the obvious binary control $b = b_{\mathrm{acm}}$. Thus, it holds $n_x = 12$ and $n_u = 2$. Further, we introduce $n_s = 7$ slack variables $\vec{s}$. The time-varying parameters are $\vec{c}^\top = [T_{\mathrm{amb}}\ \dot{Q}_{\mathrm{load}}\ I_{\mathrm{g}}]$ such that $n_c = 3$. With $\vec{v}(t)^\top = [\vec{x}(t)^\top \vec{u}(t)^\top b(t)\ \vec{s}(t)^\top]$ the vector of optimization variables and $\vec{s}(t)^\top = [\Delta T_{\mathrm{r,a}}(t)\ \vec{s}_{\mathrm{lb}}(t)^\top\ \vec{s}_{\mathrm{ub}}(t)^\top]$, the MIOCP for the STCS reads as

$$\min_{\vec{v}(\cdot)} \int_{t_0}^{t_\mathrm{f}} \vec{u}(t)^\top W_u \vec{u}(t)\,\mathrm{d}t + \int_{t_0}^{t_\mathrm{f}} \vec{s}(t)^\top W_s \vec{s}(t)\,\mathrm{d}t - w_{T_{\mathrm{hts},1}} T_{\mathrm{hts},1}(t_\mathrm{f}) + w_{T_{\mathrm{lts},3}} T_{\mathrm{lts},3}(t_\mathrm{f}) \quad (14a)$$

$$\text{s. t. for } t \in [t_0, t_\mathrm{f}]:$$

$$(1)\text{-}(9), \quad (14b)$$

$$T_{\mathrm{r,a,lb}} \le T_{\mathrm{r,a}}(t) + \Delta T_{\mathrm{r,a}}(t) \le T_{\mathrm{r,a,ub}}, \quad (14c)$$

$$\vec{\epsilon} \ge b(t) \left(\begin{pmatrix} T_{\mathrm{ht,lb}} - T_{\mathrm{hts},1}(t) \\ T_{\mathrm{lt,lb}} - T_{\mathrm{lts},1}(t) \\ T_{\mathrm{amb,lb}} - T_{\mathrm{amb}}(t) \end{pmatrix} - \vec{s}_{\mathrm{lb}}(t) \right), \quad (14d)$$

$$\vec{\epsilon} \ge b(t) \left(\begin{pmatrix} T_{\mathrm{hts},1}(t) - T_{\mathrm{ht,ub}} \\ T_{\mathrm{lts},1}(t) - T_{\mathrm{lt,ub}} \\ T_{\mathrm{amb}}(t) - T_{\mathrm{amb,ub}} \end{pmatrix} - \vec{s}_{\mathrm{ub}}(t) \right), \quad (14e)$$

$$T_{\mathrm{lb}} \le T(t) \le T_{\mathrm{ub}}, \quad \forall\, T(t) \in \vec{x}(t), \quad (14f)$$

$$\vec{u}_{\mathrm{lb}} \le \vec{u}(t) \le \vec{u}_{\mathrm{ub}}, \quad (14g)$$

$$b(t) \in \{0, 1\}, \quad (14h)$$

$$\vec{x}(t_0) = \vec{x}_0. \quad (14i)$$

The Lagrange term of the objective (14a) contains the sum of squares of continuous controls $\vec{u}$ and slack variables $\vec{s}$ weighted by appropriately chosen weightings $W_u \in \mathbb{R}^{n_u \times n_u}$ and $W_s \in \mathbb{R}^{n_s \times n_s}$, respectively. The minimization of $\vec{u}$ favors energy efficient pump use, while minimization of $\vec{s}$ reduces the deviation $\Delta T_{\mathrm{r,a}}$ of the room temperature from the comfort range $T_{\mathrm{r,a,lb}} = 21^\circ\,\mathrm{C}$ and $T_{\mathrm{r,a,ub}} = 23^\circ\,\mathrm{C}$ in (14c) as well as the use of $\vec{s}_{\mathrm{lb}}$ and $\vec{s}_{\mathrm{ub}}$ for relaxation of the temperature boundaries for ACM operation (14d) and (14e).

The Mayer term contains the final storage layer temperatures $T_{\mathrm{hts},1}(t_\mathrm{f})$ and $T_{\mathrm{lts},3}(t_\mathrm{f})$ weighted by $w_{T_{\mathrm{hts},1}}$ and $w_{T_{\mathrm{lts},3}}$, respectively, which favors to always drive the system towards a reactive configuration of high values for $T_{\mathrm{hts},1}$ and low values for $T_{\mathrm{lts},3}$, which, e. g., is especially important within later MPC applications.

The system dynamics that must be fulfilled are given in (14b). The path constraints that enforce the temperature bounds for ACM operation are formulated in (14d) and (14e) as smoothened vanishing constraints [21]. Bounds on continuous controls given in (14g) and on states given in (14f) must be fulfilled as well as the binary constraint (14h) and the initial state in (14i).

B. Software implementation

The MIOCP discretization is conducted using direct collocation with Lagrange polynomials and implemented in CasADi 3.2.0 [22] in Python. The problem is solved once using Bonmin and once using CIA. Within CIA, Ipopt is used as NLP solver. The binary approximation (12) is computed using a custom implementation of the Branch and Bound algorithm in [10] in C++ and interfaced from Python.

Within both methods, MA27 [23] is used as linear solver for Ipopt. Valid initial guesses for optimization variables are obtained by system simulations using a simple, set-point-based control scheme in OpenModelica [24] via OMPython [25]. Within all methods and solution steps, conditions determine the maximum number of switchings $\sigma_{\max} = 4$.

C. Test scenarios

For testing the control formulation and implementation, the following operation scenarios of solar irradiation I_{g} and ambient temperature T_{amb} recorded at Karlsruhe University of Applied Sciences in 2017, with an assumed, corresponding heat load $\dot{Q}_{\mathrm{load}}$ as shown in Figure 2 are considered, which are assumed known to the controller.

- S_1: Cloud-free, high solar irradiation with nearly ideal solar profile; high ambient temperature with peak shifted in relation to the solar irradiation peak.
- S_2: Cloudy, less irradiation throughout the day, irradiation peaks in the afternoon; lower peak temperatures.
- S_3: Cloudy during noon, therefore no solar irradiation peak during that time; ambient temperature lower at noon.
- S_4: Irradiation is high until noon, then drops; most of the day, ambient temperatures are below the comfort range.

Each scenario starts at midnight and lasts 24 h, with $N = 360$ equidistant control intervals of length $\Delta t = 240\,\mathrm{s}$. Within one interval, ambient conditions are assumed constant. The vector for the initial states is given as $\vec{x}_0 = [55.0\ 51.7\ 48.3\ 45\ 20\ 19\ 18\ 20\ 21.5\ 21.5\ 21.5\ 21.5]^\top\ ^\circ\mathrm{C}$.

D. Comparison of optimization results

Table III shows the quality of the solutions for (14) obtained by Bonmin and CIA on a number of key figures K. K_1 is the solution time on an Intel Core i5-4570 3.20 GHz CPU and K_2 the achieved objective value. K_3 is the mean and

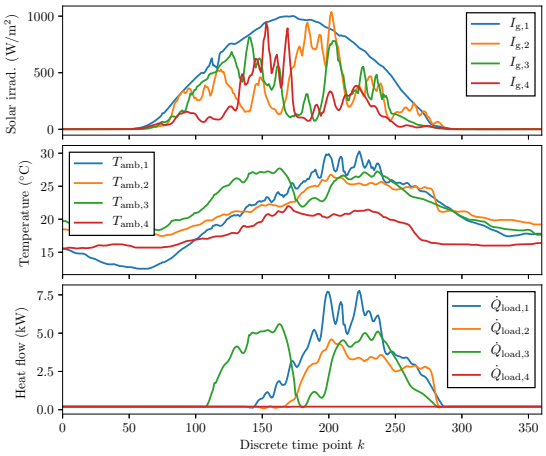

Fig. 2. Depiction of test scenarios S_1-S_4.

TABLE III

COMPARISON OF SOLUTION QUALITY OF CIA (C) AND BONMIN (B) FOR SCENARIOS S_1-S_4.

	Key figure	Unit	S_1-C	S_1-B	S_2-C	S_2-B	S_3-C	S_3-B	S_4-C	S_4-B
K_1	Solution time	s	9.39e+01	4.80e+04	5.95e+01	6.26e+04	6.07e+01	1.89e+05	6.01e+01	6.50e+02
K_2	Objective value	-	-7.93e+00	-7.94e+00	-6.76e+00	-7.46e+00	-4.12e+00	-4.89e+00	-7.14e+00	-6.03e+00
K_3	$(N+1)^{-1}\sum_{k=1}^{N+1}\Delta T_{\mathrm{r,a,k}}$	°C	-1.68e-03	-1.65e-03	-2.81e-03	-2.19e-03	-1.21e-02	-7.06e-03	2.95e-10	3.24e-12
K_4	$\max_{k=1,\dots,N+1}(\lvert\Delta T_{\mathrm{r,a,k}}\rvert)$	°C	4.76e-02	4.74e-02	5.02e-02	3.47e-02	1.48e-01	8.23e-02	6.06e-10	6.67e-12
K_5	$N^{-1}\sum_{k=1}^{N} s_{\mathrm{lb,1,k}}$	°C	8.83e-05	8.06e-05	4.09e-05	1.92e-04	3.61e-05	6.42e-06	2.15e-05	4.00e-05
K_6	$\max_{k=1,\dots,N}(\lvert s_{\mathrm{lb,1,k}}\rvert)$	°C	2.58e-03	1.39e-02	4.10e-05	2.96e-02	3.61e-05	6.42e-06	2.15e-05	4.02e-05
K_7	$N^{-1}\sum_{k=1}^{N} s_{\mathrm{lb,2,k}}$	°C	4.14e-05	1.46e-05	2.66e-03	3.97e-05	6.18e-03	2.37e-04	1.22e-04	4.00e-05
K_8	$\max_{k=1,\dots,N}(\lvert s_{\mathrm{lb,2,k}}\rvert)$	°C	1.67e-03	1.95e-03	4.06e-01	8.47e-03	2.85e-01	4.55e-02	3.61e-02	4.00e-05
K_9	$T_{\mathrm{hts},0,N+1}$	°C	1.04e+02	1.04e+02	9.78e+01	9.64e+01	8.19e+01	7.97e+01	8.80e+01	7.24e+01
K_{10}	$T_{\mathrm{lts},3,N+1}$	°C	1.65e+01	1.61e+01	2.02e+01	1.96e+01	2.01e+01	1.98e+01	1.64e+01	1.13e+01
K_{11}	$\sum_{k=1}^{N} b_{\mathrm{acm},k}\Delta t$	s	2.16e+04	2.18e+04	8.64e+03	1.01e+04	2.06e+04	2.21e+04	7.20e+02	4.32e+03
K_{12}	$\sum_{k=1}^{N} \dot{m}_{\mathrm{sc},k}\Delta t$	kg	5.04e+03	5.05e+03	4.50e+03	2.33e+03	4.94e+03	4.03e+03	7.00e+02	1.78e+03
K_{13}	$\sum_{k=1}^{N} \dot{m}_{\mathrm{fc,w},k}\Delta t$	kg	3.36e+03	3.34e+03	1.89e+03	1.70e+03	4.79e+03	4.62e+03	2.45e-04	0.00e+00

K_4 the maximum absolute deviation of the room temperature from the comfort range $\Delta T_{\mathrm{r,a}}$. K_5 to K_8 are the mean and maximum absolute values of the utilized slack variables $s_{\mathrm{lb},1}$ and $s_{\mathrm{lb},2}$. K_9 and K_{10} are the final values of $T_{\mathrm{hts},1}$ and $T_{\mathrm{lts},3}$. In K_{11} the total ACM runtime is given and in K_{12} and K_{13} the total amount of mass transported by the solar circuit pump and cooling circuit pump, respectively.

It is shown that all solution times K_1 of CIA are below 10^2 s which is a fraction of the control interval length Δt, while solution times for Bonmin are up to several orders of magnitude higher. This can be explained by the number of NLPs solved within CIA being exactly two, while within one run of Bonmin possibly several hundreds of NLPs are solved. Nevertheless, the objectives K_2 obtained by CIA are comparable to the results of Bonmin. The aim of preserving the comfort range (14c) is fulfilled well for both methods in terms of K_3 and K_4 and the final storage layer temperatures in K_9 and K_{10} are comparable. The differences in K_9 to K_{11} for S_4 show a higher utilization of ACM and driving energy from the HT storage by Bonmin to achieve a lower LT storage temperature than CIA which results in a similarly good solution for (14).

Apart from that, the differences in solutions mainly lie within different utilization of pumps and slack variables for path constraint relaxation. Reasons for this can be illustrated on a more detailed comparison of the solutions for S_2 in Figure 3. It shows that the development of system temperatures is similar, ACM operation is predictively scheduled within efficient operation conditions and the maximum switching constraint is fulfilled for both methods. However, utilization of the solar circuit pump is much higher for CIA for time points before approx. $N = 170$. This is caused by the ACM operation schedule obtained by $\mathrm{CIA}_{\mathrm{MILP}}$ from the relaxed profile of $\mathrm{CIA}_{\mathrm{NLP},1}$ that switches on the ACM relatively early compared to the profile obtained by Bonmin, which forces the optimizer in $\mathrm{CIA}_{\mathrm{NLP},2}$ to utilize more pump operation in order to establish $T_{\mathrm{hts},1} \geq T_{\mathrm{ht,lb}}$ for valid ACM

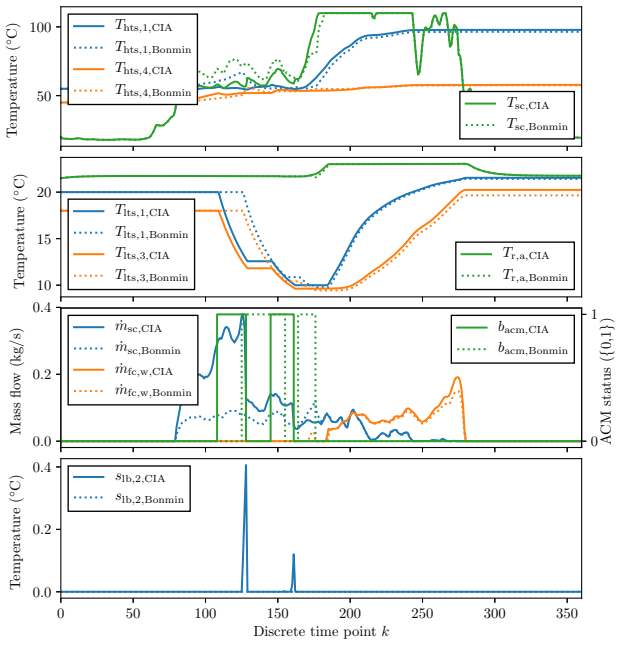

Fig. 3. Detailed depiction of solution for scenario S_2.

operation. Since the energy provided by solar irradiation is limited, the optimizer needs to temporarily decrease parts of the minimum operation conditions in (14d) by about 0.4 °C using $s_{\mathrm{lb},2}$ around approx. $N = 120$ and by about 0.1 °C around approx. $N = 170$ to preserve feasibility of the NLP.

With Bonmin, such situations do not occur since binary and continuous controls are treated simultaneously. However, in practical HVAC applications constraint violations of such dimension appear tolerable and the benefits of improved system control facilitated by shorter solution times prevail the drawback of small, temporary constraint violations. Additionally, more restrictive constraints could be chosen for the MIOCP such that small constraint violations do not violate the actual operation conditions of the controlled machinery.

E. Relation of solution time and number of control intervals

Figure 4 depicts a comparison of the solution times of Bonmin and CIA, as well as the duration of the several CIA solution steps $\mathrm{CIA}_{\mathrm{NLP},1}$, $\mathrm{CIA}_{\mathrm{MILP}}$ and $\mathrm{CIA}_{\mathrm{NLP},2}$ for different numbers of control intervals N for S_1.

The runtime increases from $N = 90$ to $N = 360$ by roughly one order of magnitude for CIA and two orders of magnitude for Bonmin. CIA runtime stays below $10^2\,\mathrm{s}$ for all tested discretizations, while the runtime of Bonmin nearly approaches $10^5\,\mathrm{s}$. The solution time of $\mathrm{CIA}_{\mathrm{MILP}}$ is very low in comparison to the NLP solutions steps, while the solution of $\mathrm{CIA}_{\mathrm{NLP},2}$ appears to take less time than solving $\mathrm{CIA}_{\mathrm{NLP},1}$. This can be reasoned by $\mathrm{CIA}_{\mathrm{NLP},2}$ being initialized with the solution of $\mathrm{CIA}_{\mathrm{NLP},1}$ and $\mathrm{CIA}_{\mathrm{MILP}}$, which is likely to be a better initialization than the one for $\mathrm{C}_{\mathrm{NLP},1}$ obtained in OpenModelica. This behavior is favorable for use of the CIA algorithm within MPC application where, after the first solution, the control problem is initialized with the optimal solution of the previous time step.

V. Conclusions and Future Work

Within this work, we presented an algorithm for mixed-integer optimal control of solar thermal climate systems with MPC-capable runtime. Compared to the general MINLP solver Bonmin, the algorithm is able to obtain solutions of similar quality at a highly reduced runtime.

Future work should focus on the introduction of multiple binary controls for the algorithm, investigations on the runtime development for increasing system sizes and application of the method for MPC of the simulated and physical system.

Acknowledgments

This research was supported by the EU via FP7-ITN-TEMPO (607 957) and H2020-ITN-AWESCO (642 682), by the Federal Ministry for Economic Affairs and Energy (BMWi) via eco4wind and DyConPV, by DFG via Research Unit FOR 2401 and GRK 2297 and by the State Ministry of Baden-Wuerttemberg for Sciences, Research and Arts (Az: 22-7533.-30-20/9/3).

References

[1] U. Berardi, "A cross-country comparison of the building energy consumptions and their trends," *Resources, Conservation and Recycling*, vol. 123, pp. 230 – 241, 2017.

[2] B. Choudhury, B. B. Saha, P. K. Chatterjee, and J. P. Sarkar, "An overview of developments in adsorption refrigeration systems towards a sustainable way of cooling," *Applied Energy*, vol. 104, pp. 554 – 567, 2013.

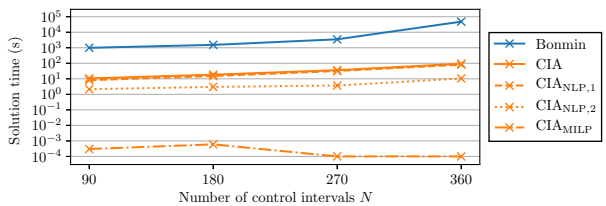

Fig. 4. Runtimes of Bonmin (B), CIA (C) and CIA solution steps $\mathrm{C}_{\mathrm{NLP},1}$, $\mathrm{C}_{\mathrm{MILP}}$ and $\mathrm{C}_{\mathrm{NLP},2}$ for different numbers of control intervals for S_1.

[3] W.-S. Chang, C.-C. Wang, and C.-C. Shieh, "Experimental study of a solid adsorption cooling system using flat-tube heat exchangers as adsorption bed," *Applied Thermal Engineering*, vol. 27, no. 13, pp. 2195 – 2199, 2007.

[4] M. Gräber, "Energieoptimale Regelung von Kälteprozessen," Ph.D. dissertation, TU Carolo-Wilhelmina zu Braunschweig, Dec 2013.

[5] U. Bau, A.-L. Braatz, F. Lanzerath, M. Herty, and A. Bardow, "Control of adsorption chillers by a gradient descent method for optimal cycle time allocation," *International Journal of Refrigeration*, vol. 56, pp. 52 – 64, 2015.

[6] A. Bürger, P. Sawant, M. Bohlayer, A. Altmann-Dieses, M. Braun, and M. Diehl, "Efficient operation scheduling for adsorption chillers using predictive optimization-based control methods," *IOP Conference Series: Materials Science and Engineering*, vol. 257, no. 1, p. 012007, 2017.

[7] S. Sager, "Reformulations and algorithms for the optimization of switching decisions in nonlinear optimal control," *Journal of Process Control*, vol. 19, no. 8, pp. 1238 – 1247, 2009, special Section on Hybrid Systems: Modeling, Simulation and Optimization.

[8] T. Binder, L. Blank, H. G. Bock, R. Bulirsch, W. Dahmen, M. Diehl, T. Kronseder, W. Marquardt, J. P. Schlöder, and O. von Stryk, *Online Optimization of Large Scale Systems*. Springer Berlin Heidelberg, 2001, ch. Introduction to Model Based Optimization of Chemical Processes on Moving Horizons, pp. 295 – 339.

[9] P. Bonami, L. T. Biegler, A. R. Conn, G. Cornuéjols, I. E. Grossmann, C. D. Laird, J. Lee, A. Lodi, F. Margot, N. Sawaya, and A. Wächter, "An algorithmic framework for convex mixed integer nonlinear programs," *Discrete Optimization*, vol. 5, no. 2, pp. 186 – 204, 2008.

[10] S. Sager, M. Jung, and C. Kirches, "Combinatorial Integral Approximation," *Mathematical Methods of Operations Research*, vol. 73, no. 3, pp. 363–380, 2011.

[11] M. Jung, "Relaxations and Approximations for Mixed-Integer Optimal Control," Ph.D. dissertation, Interdisciplinary Center for Scientific Computing, Heidelberg University, 2013.

[12] B. Joseph-Duran, M. N. Jung, C. Ocampo-Martinez, S. Sager, and G. Cembrano, "Minimization of sewage network overflow," *Water Resources Management*, vol. 28, no. 1, pp. 41–63, 2014.

[13] S. Sager, M. Claeys, and F. Messine, "Efficient upper and lower bounds for global mixed-integer optimal control," *Journal of Global Optimization*, vol. 61, no. 4, pp. 721–743, 2015.

[14] L. Biegler, *Nonlinear Programming*. Society for Industrial and Applied Mathematics, 2010.

[15] V. Wesselak, T. Schabbach, T. Link, and J. Fischer, *Regenerative Energietechnik*, 2nd ed. Berlin, Heidelberg: Springer Vieweg, 2013.

[16] G. Streckiene, V. Martinaitis, and P. Vaitiekunas, "Simulation of thermal stratification in the heat storage for CHP plant," in *8th International Conference on Environmental Engineering*, 2011.

[17] U. Eicker, *Solar technologies for buildings*. Chichester: John Wiley & Sons, 2003.

[18] P. A. Sawant and J. Pfafferott, "Experimental investigation of a real-life microscale trigeneration system using adsorption cooling, reversible heat-pump and a cogeneration unit," in *7th International Conference on Experiments/Process/System Modeling/Simulation/Optimization IC-EPSMSO*, 2017.

[19] P. Belotti, C. Kirches, S. Leyffer, J. Linderoth, J. Luedtke, and A. Mahajan, "Mixed-integer nonlinear optimization," *Acta Numerica*, vol. 22, p. 1131, 2013.

[20] A. Wächter and L. T. Biegler, "On the implementation of an interior-point filter line-search algorithm for large-scale nonlinear programming," *Mathematical Programming*, vol. 106, no. 1, pp. 25–57, 2006.

[21] M. Jung, C. Kirches, and S. Sager, "On Perspective Functions and Vanishing Constraints in Mixed-Integer Nonlinear Optimal Control," in *Facets of Combinatorial Optimization*, M. Jünger and G. Reinelt, Eds. Springer Berlin Heidelberg, 2013, pp. 387–417.

[22] J. Andersson, "A General-Purpose Software Framework for Dynamic Optimization," Ph.D. dissertation, KU Leuven, October 2013.

[23] HSL, "A collection of fortran codes for large scale scientific computation," 2017. [Online]. Available: http://www.hsl.rl.ac.uk/

[24] The Open Source Modelica Consortium, "OpenModelica," 2017. [Online]. Available: https://www.openmodelica.org

[25] B. Lie, S. Bajracharya, A. Mengist, L. Buffoni, A. Palanisamy, M. Sjölund, A. Asghar, A. Pop, and P. Fritzson, "API for accessing OpenModelica models from Python," in *Proceedings of 9th EUROSIM Congress on Modelling and Simulation*, Sept. 2016.